

SPECIAL**Advances in Drought Monitoring****COLLECTION**

Probabilistic Seasonal Forecasting of African Drought by Dynamical Models

XING YUAN, ERIC F. WOOD, NATHANIEL W. CHANEY, JUSTIN SHEFFIELD, JONGHUN KAM,
MIAOLING LIANG, AND KAIYU GUAN

Department of Civil and Environmental Engineering, Princeton University, Princeton, New Jersey

(Manuscript received 3 April 2013, in final form 20 June 2013)

ABSTRACT

As a natural phenomenon, drought can have devastating impacts on local populations through food insecurity and famine in the developing world, such as in Africa. In this study, the authors have established a seasonal hydrologic forecasting system for Africa. The system is based on the Climate Forecast System, version 2 (CFSv2), and the Variable Infiltration Capacity (VIC) land surface model. With a set of 26-yr (1982–2007) seasonal hydrologic hindcasts run at 0.25°, the probabilistic drought forecasts are validated using the 6-month Standard Precipitation Index (SPI6) and soil moisture percentile as indices. In terms of Brier skill score (BSS), the system is more skillful than climatology out to 3–5 months, except for the forecast of soil moisture drought over central Africa. The spatial distribution of BSS, which is similar to the pattern of persistency, shows more heterogeneity for soil moisture than the SPI6. Drought forecasts based on SPI6 are generally more skillful than for soil moisture, and their differences originate from the skill attribute of resolution rather than reliability. However, the soil moisture drought forecast can be more skillful than SPI6 at the beginning of the rainy season over western and southern Africa because of the strong annual cycle. Singular value decomposition (SVD) analysis of African precipitation and global SSTs indicates that CFSv2 reproduces the ENSO dominance on rainy season drought forecasts quite well, but the corresponding SVD mode from observations and CFSv2 only account for less than 24% and 31% of the covariance, respectively, suggesting that further understanding of drought drivers, including regional atmospheric dynamics and land–atmosphere coupling, is necessary.

1. Introduction

Drought is a natural phenomenon due to climate variability. However, with global warming and population growth, the resilience to drought is likely to decrease in the future. Unlike other meteorological hazards such as floods, tornados, and hurricanes, drought is a creeping phenomenon that can build up without warning and persist for many months (Sheffield and Wood 2011). Once the water deficit of the climate system reaches a certain threshold, drought will affect agriculture, water supply, and the environment, often with devastating impacts. In the developed world, drought is generally associated with crop yield declines, environmental degradation, and corresponding economic losses. In the developing world, such as most of Africa, drought can be

a severe threat to the local population through loss of livelihoods, food insecurity, and famine. For example, the 2010–11 drought in the Horn of Africa affected about 12 million people, which led to severe food shortages in parts of Ethiopia, Djibouti, Somalia, and northern Kenya. The related population displacement and price increase of food and fuel resulted in a serious humanitarian crisis (Dutra et al. 2012; Peterson et al. 2012). Therefore, the provision of seasonal forecasts that can provide sufficient early warning has the potential to help the local governments and nongovernmental organizations (NGOs) to move from management of drought crises to management of drought risk, increasing the resilience to drought events, and reducing the possibility of humanitarian crises (Pozzi et al. 2013).

The major source of seasonal forecast predictability comes from the ocean, and the strongest signal is the El Niño–Southern Oscillation (ENSO). As the easterly trade winds weaken, sea surface temperatures (SSTs) in the eastern tropical Pacific increase. This alters the Walker circulation and the convection zone in the tropics,

Corresponding author address: Xing Yuan, Department of Civil and Environmental Engineering, Princeton University, E318 Engineering Quad, Princeton, NJ 08544.
E-mail: xingy@princeton.edu

affecting the climate in midlatitudes and high latitudes through Rossby wave trains (Hoskins and Karoly 1981; Trenberth and Caron 2000). For example, composite analysis indicates that there is a greater chance of drought over western Africa and southern Africa during their respective rainy seasons during El Niño years than during La Niña years (Smith et al. 2012). Besides ENSO, a warm South Atlantic will lower the thermal gradient with the African continent, resulting in a southward shift of the intertropical convergence zone (ITCZ), with corresponding drought in the Sahel region (Camberlin et al. 2001). Recently, the Indian Ocean and Mediterranean Sea are receiving more attentions for their contributions to the rainfall variability over eastern and northern Africa, respectively (Bowden and Semazzi 2007; Gimeno et al. 2012). These teleconnections have been used to form the basis for developing statistical approaches in forecasting drought at seasonal scales (Barnston et al. 1996; Mason 1998). On the other hand, atmosphere–ocean–land coupled general circulation models (CGCMs), developed based on the Navier–Stokes equations and parameterizations that characterize the water and energy exchanges among the land, atmosphere, and ocean, are beginning to outperform statistical models for ENSO prediction skill (Barnston et al. 2012). This is mainly because of gradual improvements in observations and assimilation systems, physical parameterizations, spatial resolution, and understanding of ENSO-related ocean–atmosphere interactions (Barnston et al. 2012). Thus, we expect CGCMs would provide more dynamical and objective drought forecasts for land regions such as Africa and the transition of advances in climate research to climate services.

In fact, CGCM-based seasonal forecasting of drought has become operational in recent years at many national weather centers. Several previous studies have used these operational systems to hindcast specific drought events (Luo and Wood 2007; Yuan et al. 2011; Dutra et al. 2012), while other work has systematically evaluated drought forecast skill using a set of hindcast experiments (Mo et al. 2012; Yoon et al. 2012; Yuan et al. 2013). The CGCM-based drought forecasting approach can be divided in two steps. First, meteorological forcings from the CGCM forecasts are bias corrected and downscaled to the resolution that is suitable for regional applications, with the resulting precipitation used to calculate a meteorological drought index, such as the Standardized Precipitation Index (SPI; McKee et al. 1993, 1995). Second, the downscaled meteorological forcings are used to force well-calibrated land surface hydrologic models to resolve terrestrial water and energy variations, with the predicted land surface conditions, such as soil moisture and streamflow, used to

derive agricultural and hydrological drought indices (Luo and Wood 2007; Mo et al. 2012; Yuan et al. 2013). Most of the previous forecasting studies have focused on a single type of drought, such as meteorological drought or agricultural drought, and have mainly focused on the ensemble mean values to make deterministic assessments (Mo et al. 2012; Yuan et al. 2013). There is, therefore, a need to compare different drought indices to understand the forecast skill in different parts of the hydrological cycle that are important for different activities and their relationships and to investigate the probabilistic characteristics of the drought forecasts.

In this paper, we use the National Centers for Environmental Prediction's (NCEP) Climate Forecast System, version 2 (CFSv2; Saha et al. 2013), combined with the Variable Infiltration Capacity (VIC; Liang et al. 1996) land surface model for seasonal drought prediction over Africa—a region that has a preponderance of severe droughts and associated impacts and the potential for more resilient livelihoods through use of seasonal forecasts (Tarlule and Lamb 2003; Batté and Déqué 2011; Dutra et al. 2012; Landman et al. 2012). Both the SPI and soil moisture percentiles are used as indices to assess probabilistic drought hindcasts for 1982–2007. The hindcast setup and evaluation methods are described in section 2. The results are presented in section 3, and a discussion and summary are given in sections 4 and 5, respectively.

2. Hindcast setup and evaluation method

Before calculating the SPI or running the VIC model over Africa, we downscale the CFSv2 monthly precipitation and temperature hindcasts for 1982–2007 from T126 resolution to 0.25° . The CFSv2 hindcast is initiated every 5 days with four cycles on those days, resulting in 24 ensemble members (Yuan et al. 2011), which is different from its real-time forecast that is being initiated every 6 h with up to 124 ensemble members. Different combinations of ensemble members might result in different climate variability of the model. Therefore, caution should be taken before applying the following downscaling procedures to real-time drought forecast. In this study, the downscaling procedure is similar to Yuan et al. (2013), which is based on the Bayesian merging method of Luo et al. (2007). The observational dataset used for correcting the hindcasts is a new 0.25° , daily resolution dataset (Sheffield et al. 2013, manuscript submitted to *Bull. Amer. Meteor. Soc.*) that extends the work of Sheffield et al. (2006). Basically, the 1° daily precipitation data from Sheffield et al. (2006) are bilinearly interpolated into 0.25° and then rescaled by using the University of East Anglia Climate Research Unit (CRU)

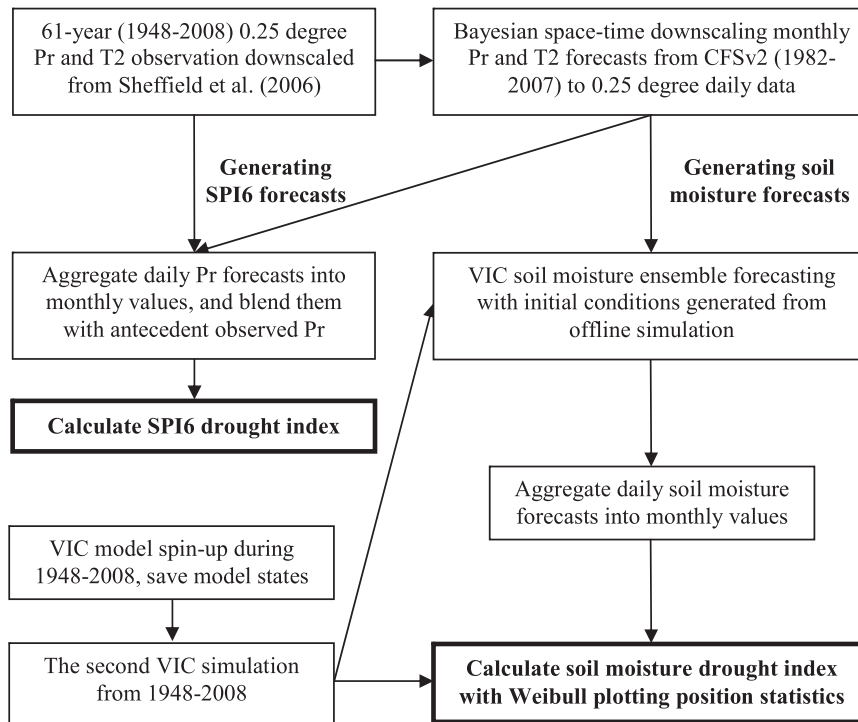


FIG. 1. Flowchart of hindcast setup and data processing.

monthly gridded gauge analysis. The daily temperature data of Sheffield et al. (2006) are also interpolated into 0.25° , but with consideration of elevation effects. With the Bayesian downscaled monthly precipitation and temperature forecasts, a hybrid method that includes both the historical-analog criterion and random selection is used to generate 20 daily time series with a scaling method to correct sampling errors (Yuan et al. 2013).

The downscaled daily precipitation datasets are then aggregated back to monthly values, and the 6-month SPI (SPI6) is calculated for the 20 ensembles (see Fig. 1 for the flowchart). We then blend the 6-month precipitation forecast with antecedent observations to obtain SPI6 at different forecast lead times. For example, for the month 1 forecast starting from June 1982, we blend the precipitation observation from January to May in 1982 with the June precipitation forecast to obtain the 6-month moving average precipitation and convert this to SPI6 for June based on the 30-yr, 6-month (January–June during 1952–81) moving average precipitation from the historical record; for the month 2 forecast, we use 2-month forecasts (June and July) and calculate the corresponding SPI6 for July, and so on. Therefore, the SPI6 forecast from month 1 to month 5 contains information from antecedent observations, which can be considered as initial condition information similar to soil moisture in hydrological forecasts.

In the second step, the downscaled daily meteorological forcings are used to drive the hydrologic model simulations to provide agricultural or hydrological drought forecasts. We use a calibrated version of the VIC model that is developed for the Princeton African Drought Monitor system (hydrology.princeton.edu/monitor; Sheffield et al. 2013, manuscript submitted to *Bull. Amer. Meteor. Soc.*). The model is calibrated using streamflow observations from over 800 Global Runoff Data Centre (GRDC) gauges, which cover most of western Africa and parts of eastern and southern Africa. On average, the calibration increases the Nash–Sutcliffe efficiency coefficients from -0.54 to 0.66 for monthly streamflow simulations (Sheffield et al. 2013, manuscript submitted to *Bull. Amer. Meteor. Soc.*). The annual mean evapotranspiration (ET) and change in seasonal water storage are compared with an energy-budget-based satellite ET product and Gravity Recovery and Climate Experiment (GRACE) satellite data, respectively, and overall, they show consistency (Sheffield et al. 2013, manuscript submitted to *Bull. Amer. Meteor. Soc.*). Although there is no direct measurement for validating soil moisture, we assume that the calibrated VIC model would produce reasonable soil moisture simulation given successful modeling of streamflow, ET, and terrestrial water storage change mentioned above. The initial conditions for the hindcasts are generated as

follows. First, we run the VIC model from 1948 to 2008 with default initial conditions. Next, we save the model states at the end of the run, use these as initial conditions on 1 January 1948, run the model from 1948 to 2008 again, and save the states during 1982–2007 at the beginning of each calendar month. These initial states are used to initialize the hydrological hindcasts.

The VIC model seasonal drought hindcast runs consist of 6-month, 20-member ensemble soil moisture hindcasts over Africa at 0.25° , daily resolution, starting on the first day of each calendar month during 1982–2007. As described in Yuan et al. (2013), the raw CFSv2 hindcast data have 24 ensemble members, with some ensemble members being about 20 days old at the beginning of the target month. Therefore, hereafter, we call the month 1 forecast as the forecast at 0.5-month lead time, month 2 as the forecast at 1.5-month lead, and so on. The soil moisture forecasts are converted to percentiles based on the 61-yr (1948–2008) climatology from the historical, observation-driven simulation. The calculated SPI6 and soil moisture percentile data are used as indices to assess the predictability of drought over Africa. Based on Svoboda et al. (2002), the thresholds for moderate and extreme drought are chosen as -0.8 and -1.6 for SPI6 and 20% and 5% for soil moisture percentile, respectively.

To assess the probabilistic forecasts of drought events, we use the Brier score (BS) defined as (Wilks 2011)

$$\text{BS} = \frac{1}{n} \sum_{k=1}^n (y_k - o_k)^2, \quad (1)$$

where k denotes a number of n events of forecast–observation pairs, y_k is the probability of drought occurrence from forecast for the k th event, and o_k is the corresponding probability from the observations with $o_k = 1$ if the drought event occurs and $o_k = 0$ if it does not. Based on the probability of the conditional distribution $p(o_1 | y_i)$, the BS can be decomposed into three components (Wilks 2011) as follows:

$$\begin{aligned} \text{BS} &= \frac{1}{n} \sum_{i=1}^I N_i (y_i - \bar{o}_i)^2 - \frac{1}{n} \sum_{i=1}^I N_i (\bar{o}_i - \bar{o})^2 \\ &\quad + \bar{o}(1 - \bar{o}) = \text{Rel} - \text{Res} + \bar{o}(1 - \bar{o}), \end{aligned} \quad (2)$$

where I is the discrete number of allowable forecast values (here $I = 21$ because there are 20 ensembles and the forecast value ranges from $y_1 = 0.0$ to $y_{21} = 1.0$), N_i is the number of times each forecast value y_i [$=(i-1)/20$] is used in the collection of forecasts being verified, \bar{o}_i is the conditional distribution of an observation defined as

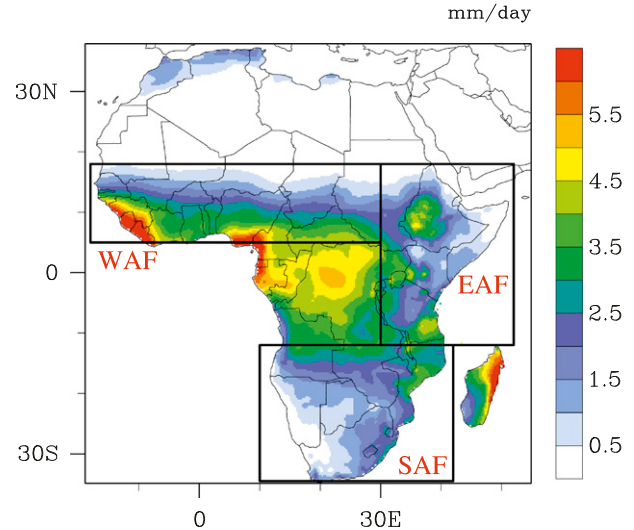


FIG. 2. Annual mean precipitation climatology during 1948–2008.

$$\bar{o}_i = p(o_1 | y_i) = \frac{1}{N_i} \sum_{k \in N_i} o_k, \quad (3)$$

and $\bar{o} = (1/n) \sum_{i=1}^I N_i p(o_1 | y_i) = (1/n) \sum_{k=1}^n o_k$. The first term of Eq. (2) is called the reliability (Rel), which measures how close the issued forecast y_i is to the probability of an observed occurrence conditional on the forecast; the second term is the resolution (Res), which refers to the differences between the conditional distributions of the observations for different forecast values; and the third term is the uncertainty (Wilks 2011). A good forecast has low Rel and high Res values.

By using the climatological forecasts as the reference, a Brier skill score (BSS) is calculated as (Wilks 2011)

$$\text{BSS} = 1 - \text{BS}/\text{BS}_{\text{clim}}; \quad (4)$$

BSS = 1 indicates a perfect forecast, while BSS less than zero means the forecast is worse than a forecast based on climatology.

3. Results

Figure 2 shows the observed 61-yr (1948–2008) mean annual precipitation over Africa, and Fig. 3 shows the area-averaged annual cycle for the terrestrial water budget simulated by VIC model except for precipitation. The precipitation has strong seasonality over the Sahel and southern Africa. For example, monthly precipitation for western Africa (WAF) and southern Africa (SAF) ranges from less than 0.5 mm day^{-1} during their dry seasons, to up to $4\text{--}6 \text{ mm day}^{-1}$ during their rainy seasons (Figs. 3b,d). In central Africa, persistent

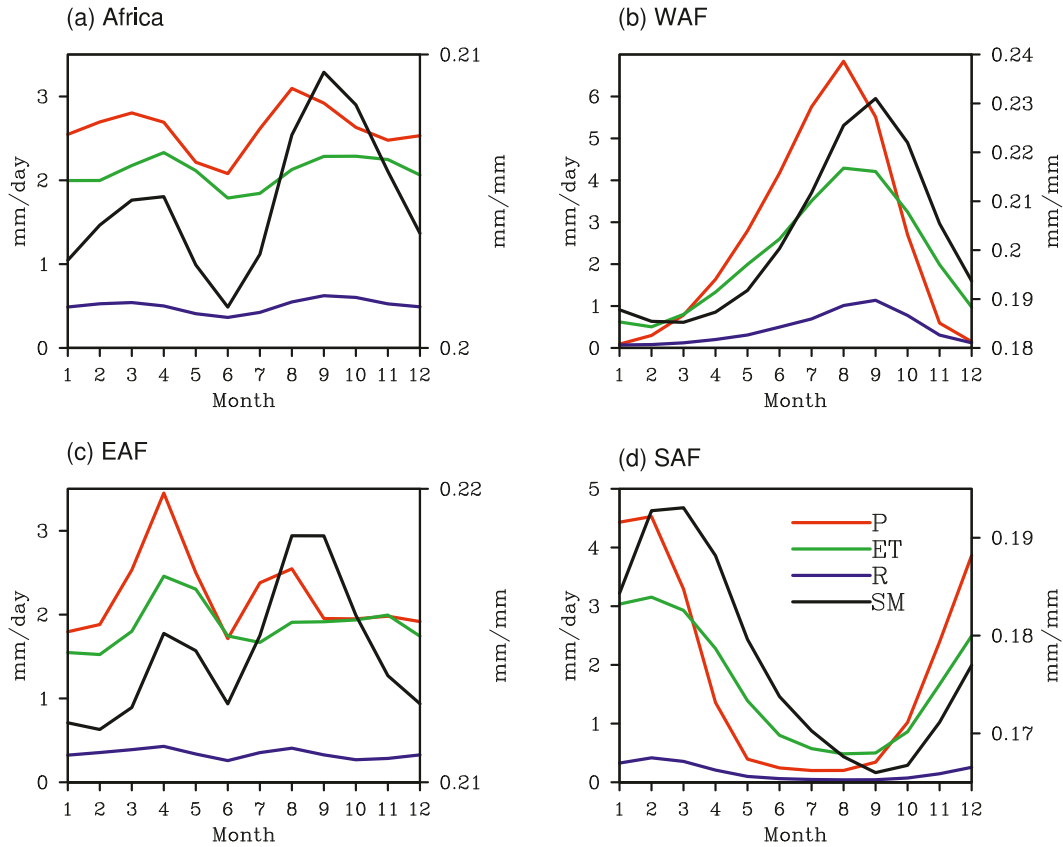


FIG. 3. Annual cycle for terrestrial precipitation (P ; mm day^{-1}), evapotranspiration (ET ; mm day^{-1}), runoff (R ; mm day^{-1}), and soil moisture (SM ; mm mm^{-1}) averaged over Africa and the three subdomains defined in Fig. 2.

precipitation generally occurs across all seasons and sustains the tropical rain forests. Eastern Africa (EAF), though situated across the equator similarly to central Africa, has a much drier climatology (Fig. 2) that is characterized by a savanna (grass and shrub) landscape.

Figure 3 also shows that the annual cycle of VIC simulated soil moisture lags behind the precipitation over WAF and SAF. The WAF is characterized by a monsoon climate, which results from the seasonal shifts of the ITCZ with a large temperature and humidity gradient between the Sahara and the tropical Atlantic Ocean. The west African monsoon migrates northward from the tropical Atlantic in February and reaches WAF near the end of June. The precipitation increases from May, reaches its peak in August (Fig. 3b), and then declines because of the retreat of the monsoon. Because of the trade-off between precipitation and ET, the soil moisture reaches its peak in September and decreases to its lowest value in March, which is 2 months after the lowest precipitation. The ITCZ also influences the northern part of SAF, while the south Indian convergence zone (SICZ; Cook 2000) plays a more important role in the

southern part of SAF. For EAF, there are two rainy seasons, but there is no obvious time lag for the soil moisture due to insufficient rainfall to compensate for ET (Fig. 3c). Later, we show how the different characteristics of the seasonality greatly affect the drought predictive skill.

Figure 4 shows the BSS for forecasts of moderate drought using SPI6 (<-0.8) and soil moisture percentile ($<20\%$), where the areas with annual mean precipitation less than 0.5 mm day^{-1} are masked out. The climatological ensemble forecast for BSS is generated by randomly sampling 20 scenarios of SPI6 or soil moisture from the 61-yr historical data pool for each calendar month, without selecting the target year. With several months of initial conditions from the observations, the SPI6 forecast at 0.5-month lead has a BSS of about 0.5–0.7 across Africa, and the value steadily declines to 0.2–0.4 at 2.5-month lead (Fig. 4). Compared to SPI6, the predictive skill for the soil moisture drought index shows more spatial heterogeneity. It has higher skill over the northern edge of WAF and parts of EAF and SAF and lower skill in central Africa, where the forecast is worse than climatology after 1 month (Fig. 4).

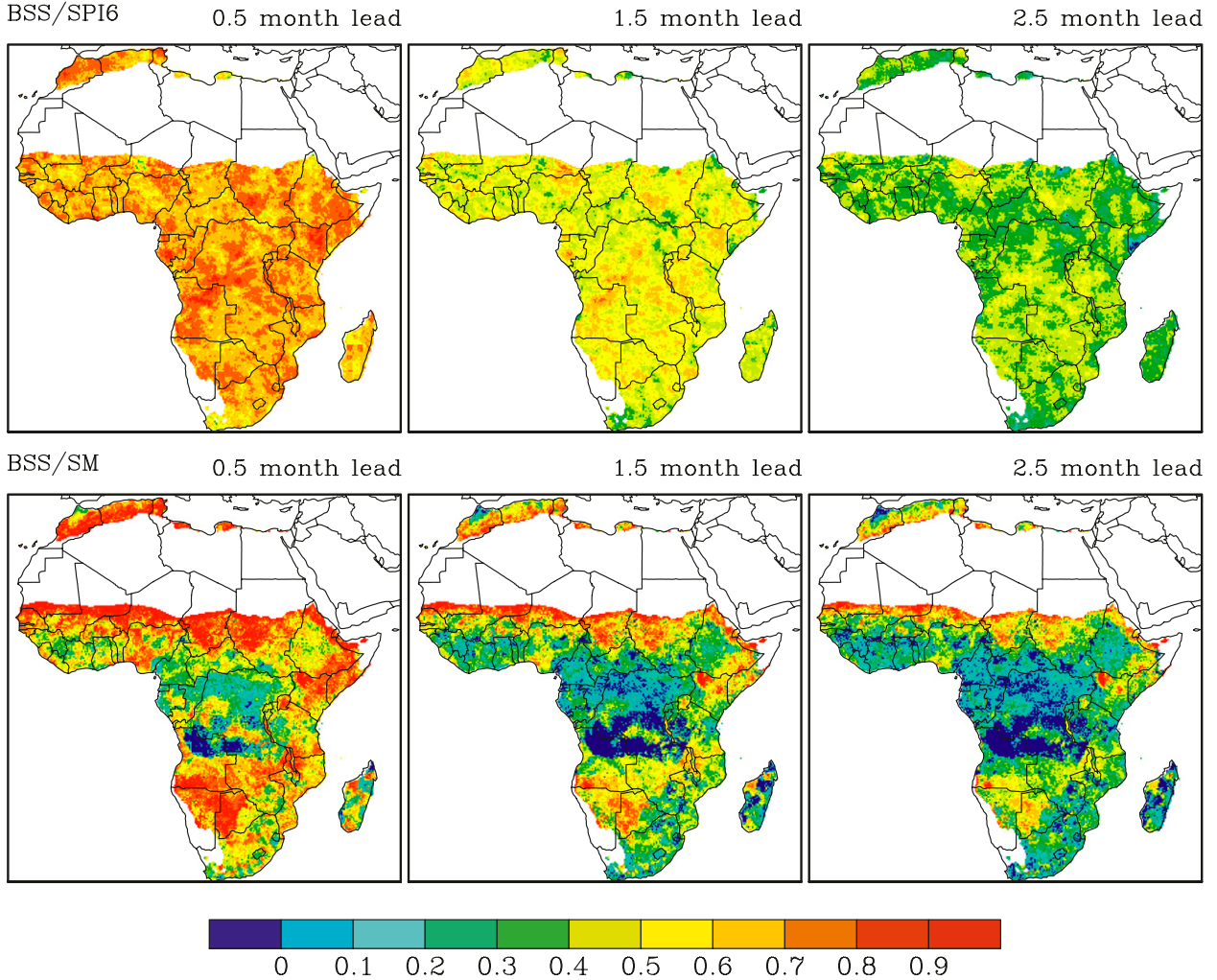


FIG. 4. BSS for moderate drought forecast at different leads for SPI6 and soil moisture percentile during 1982–2007.

To diagnose the skill difference between SPI6 and soil moisture drought forecasts probabilistically, we plot the difference in Brier score and its decomposition in Fig. 5. It is found that the forecast reliability for SPI6 and soil moisture is quite similar, but the former has higher resolution than the latter over most of the study domain out to 4 months. Since the resolution refers to the degree to which the forecasts sort the observed events into groups that are different from each other (Wilks 2011), we speculate that over tropical Africa (15°S – 15°N) and the eastern part of SAF (Fig. 5), the probability of observed drought events conditional on different soil moisture probabilistic forecast values is more similar to each other than those conditional on the SPI6 probabilistic forecast values. For example, when we check the lower tercile of the conditional distribution $p(o_1 | y_i)$ for the grid point at $(18.125^{\circ}\text{E}, 2.125^{\circ}\text{N})$, the SPI6 has a better conditional probability variations from 0 to 0.42, while

the soil moisture forecast probability varies only between 0.15 and 0.27.

To explore the reason for spatial differences in the predictive skill, we calculate the characteristic time T_0 (Trenberth 1984) for SPI6 and soil moisture from the autocorrelation $R(t)$ at lag t (months) as follows:

$$T_0 = 1 + 2 \sum_{t=1}^n (1 - t/n) R(t), \quad (5)$$

where $n = 30$ (Mo et al. 2012). T_0 can be used as a measure of persistence or memory. Figure 6 shows that the characteristic time explains the skill difference quite well. The soil moisture has longer persistence than the SPI6 (Fig. 6) over the north edge of WAF, eastern part of EAF, and western part of SAF, where the predictive skill (Fig. 4) and resolution (Fig. 5) are higher for soil

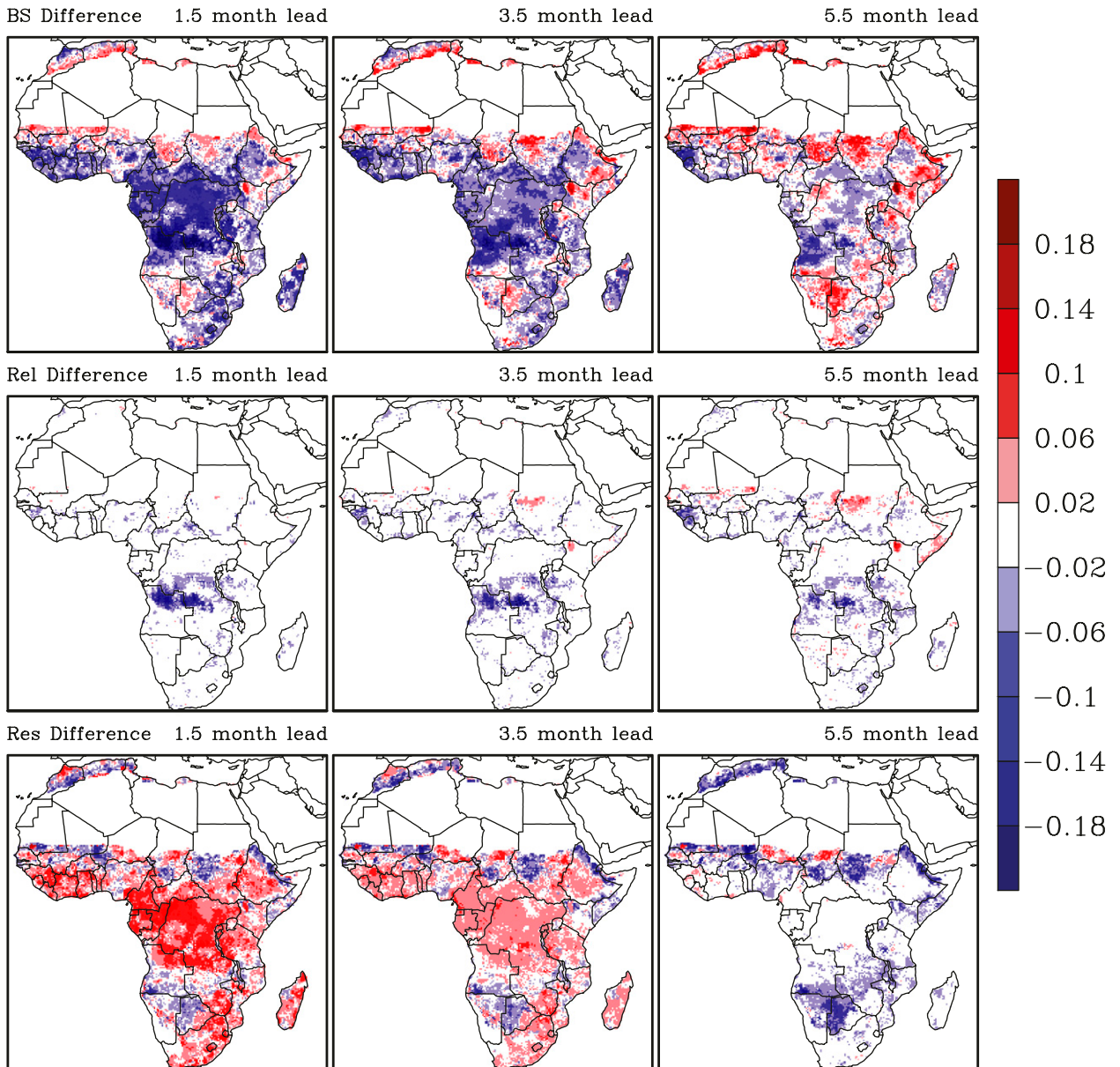
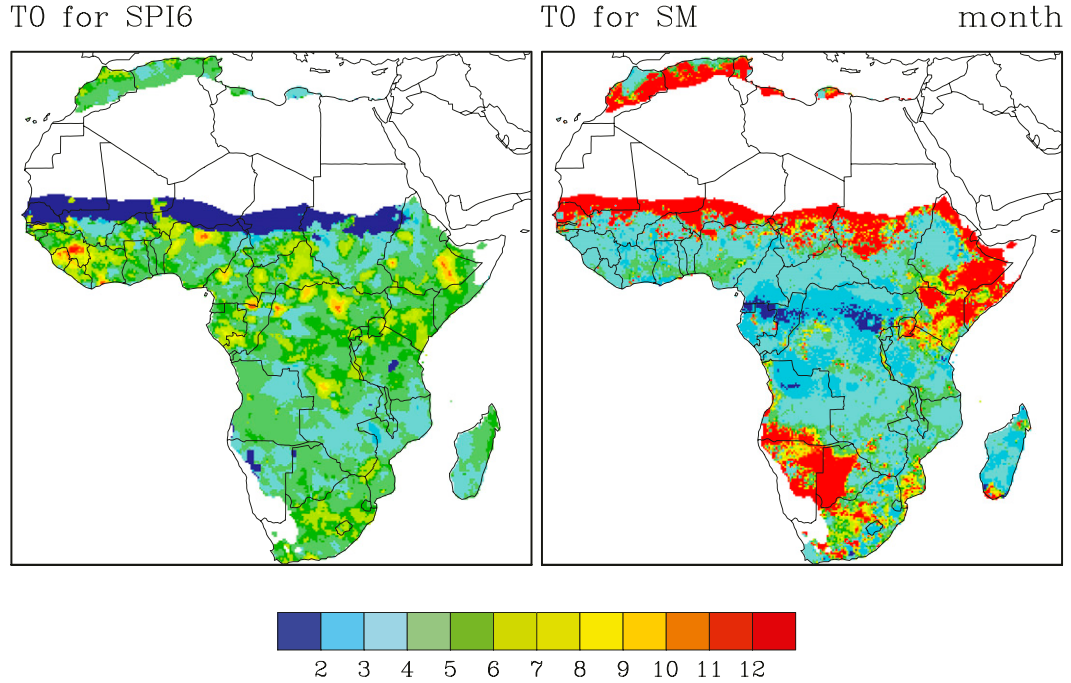


FIG. 5. Differences in BS and the decompositions (Rel and Res) for moderate drought forecast at different leads between SPI6 and soil moisture percentile.

moisture forecasts, especially for the forecasts at long leads. In contrast, the soil moisture over tropical Africa has shorter persistence than SPI6 and results in lower predictive skill.

The above predictive skill analyses are based on the statistics across all seasons. Actually, the WAF and SAF have quite different climates between dry and wet seasons, as we mentioned before. Thus, it is necessary to investigate the skill dependency by season. Although the skill difference between the SPI6 and soil moisture drought forecasts is large over tropical Africa, we

neglect this region for further analysis since it has sufficient rainfall with low interannual variability and little severe drought occurrence. Figure 7 shows the BSS averaged over the three subdomains in different seasons and the difference between SPI6 and soil moisture drought forecasts. The forecast lead in months is along the y axis and the target or verification month is along the x axis, so the value of July with 1.5-month lead is the predictive skill for July drought area from the forecast that is initiated in June (Yuan et al. 2013). In general, the drought predictive skill is higher during the dry

FIG. 6. Characteristic time (T_0) for SPI6 and soil moisture.

season and lower during the rainy season, which is expected since the hydroclimate has longer persistence during the dry season. The skill contrast between the wet/dry seasons is more obvious over WAF and SAF than EAF.

For the WAF, the wettest 6 months are from May to October, while November to April is the dry season (Fig. 3b). The SPI6 forecasts have higher skill than soil moisture drought forecasts during the dry season and the tail of the rainy season for leads up to 5 months (Fig. 7, top row). This is because, during these periods, the SPI6 has a large memory from previously observed precipitation because of its magnitude, and it affects the predictive skill directly. Although the prior precipitation anomaly information results in a soil moisture anomaly and propagates its memory, its impact on a forecast is indirect and much lower for the soil moisture drought forecast due to the uncertainty from ET and runoff estimation that can change the soil moisture. On the contrary, the soil moisture drought forecasts are better than the SPI6 forecasts at the beginning of the rainy season (Fig. 7, top row and right column), which are due to the limited magnitude and memory for rainfall before the rainy season. Similar skill difference also occurs over SAF, another region with a long rainy season, but has an austral climate. The EAF has two rainy seasons (Fig. 3c), and therefore, the SPI6 forecasts have consistently higher skill than soil moisture drought forecast out to 4 months, although the former is worse than the latter

beyond 4 months (Fig. 7, second row). This is partly because the soil moisture has longer persistence than the SPI6 over most areas of EAF (Fig. 6).

To test the capability in forecasting extreme drought events, we select two severe droughts identified by Sheffield et al. (2009) using severity-area-duration analysis. The first is the 1982–84 drought, which began in SAF at the end of 1982, migrated northwest and reached the Sahel region at the end of 1983, and persisted over the Sahel until 1986. The second severe drought affected SAF during 1991–92 for about 10 months. Following Sheffield et al. (2009), we plot the probability of drought occurrence from observations and forecasts in Fig. 8 for the most severe months: August 1984 and February 1992. Both months are in the rainy season for the Sahel and SAF, respectively. With the moderate drought threshold, the forecast probability is as high as 90% for a 1-month lead, indicating very confident drought forecasts. For a 2-month lead forecast, the probability is still larger than 60% over most of the drought area. However, with the extreme drought threshold (SPI6 < -1.6), the forecast has very low confidence (Fig. 8, second and fourth columns) even in the first month.

4. Discussion

Given the limited skill in the rainy seasons (Figs. 7, 8), the time series of rainy season mean precipitation anomaly averaged over three subdomains are shown in Fig. 9.

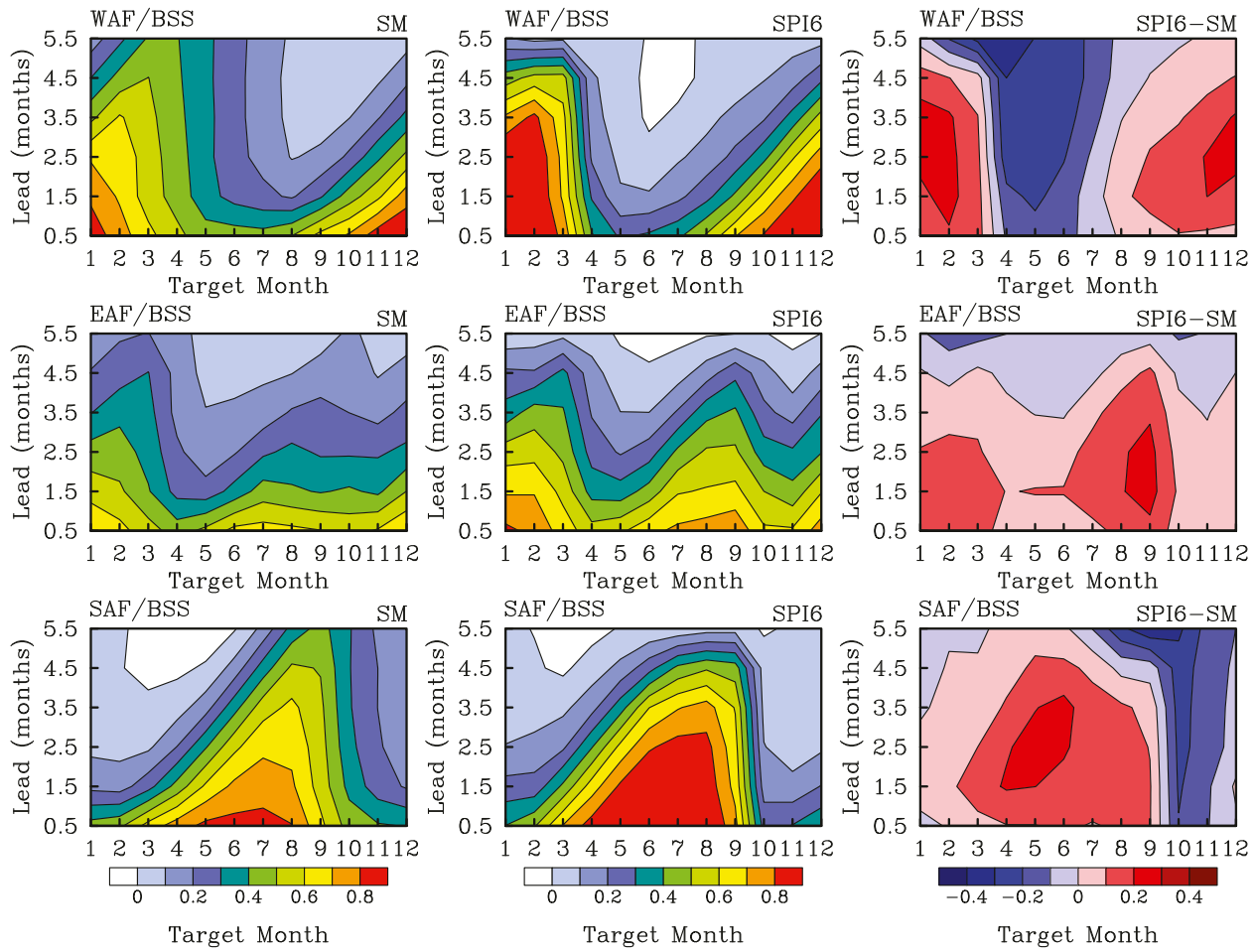


FIG. 7. BSS for SPI6 and soil moisture and their differences calculated over subdomains (Fig. 1) as functions of target months and leads.

Those anomalies are calculated from raw CFSv2 forecasts without downscaling. The rationale for checking the original time series is that the statistically downscaling method used in this paper would not improve interannual variability, similar to many other statistical downscaling methods that only use precipitation as the predictor. Consistent with Batté and Déqué (2011), who evaluated the rainy season mean precipitation predictability from multiple climate forecast models, here CFSv2 has a higher correlation over SAF than WAF (Figs. 9b,d), but it only accounts for 44%–45% of the variance of observations. For the two extreme drought cases (Fig. 8), CFSv2 predicts neutral condition or a weak anomaly (Figs. 9b,d). Therefore, all predictive skill comes from the initial condition, where its impact disappears quickly after 1 month (Fig. 8). For the EAF, March–May (MAM) is the long rainy season, and CFSv2 explains higher observed variance (53%) than the September–November (SON) short rainy season (37%). However,

CFSv2 has lower correlation during the long rainy season (Figs. 9a,c). To improve the predictability and skill for the rainy season precipitation forecasts, further effort should be devoted to conducting multimodel ensemble (Batté and Déqué 2011) and/or teleconnecting precipitation variations to more predictable climate variables such as SST.

As is well known, large-scale persistent SST anomalies are associated with long-term widespread drought (Hoerling and Kumar 2003; McCabe et al. 2004; Schubert et al. 2004, 2009). However, their relationship is more uncertain at short-term scales such as seasonal scales. To explore the covariability between African precipitation and global SSTs from both observation and CFSv2, we carry out a singular value decomposition (SVD; Bretherton et al. 1992; Wallace et al. 1992) analysis. The observed SST data are from the Extended Reconstructed Sea Surface Temperature, version 3b (ERSST v3b; Smith et al. 2008), at 2° resolution. The

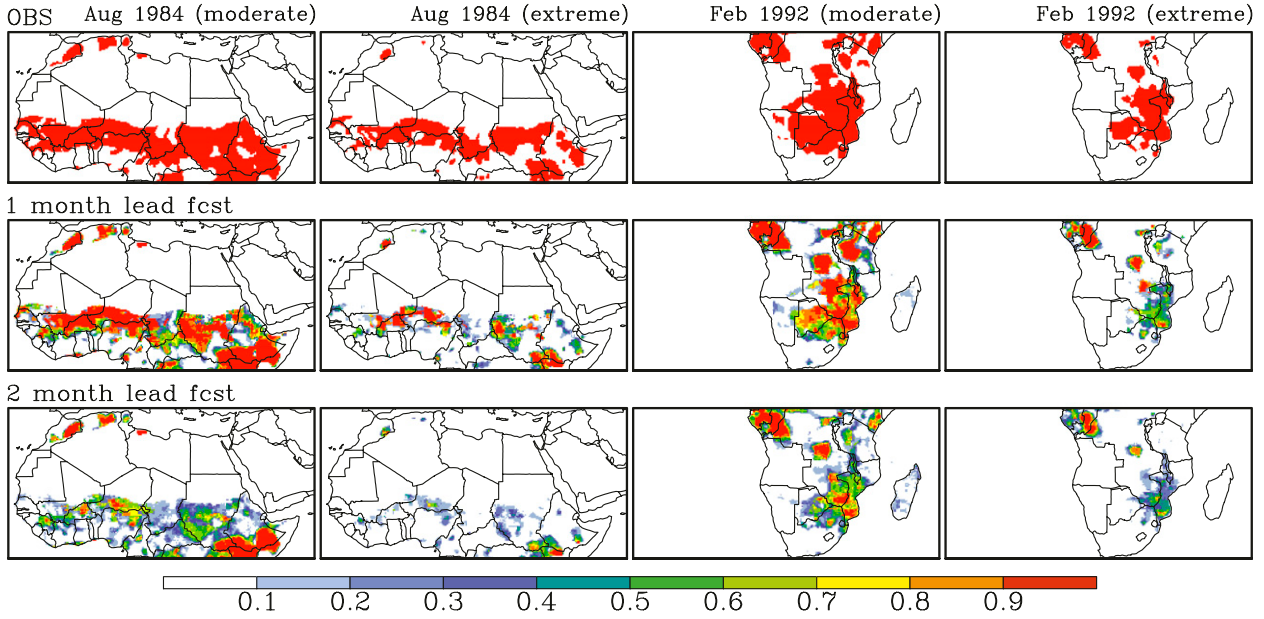


FIG. 8. Probability of drought occurrence from observation and SPI6 forecasts for two extreme drought events.

observed precipitation data, as we mentioned in section 2, are at 0.25° resolution. To facilitate data processing, we regrid CFSv2 0.5-month lead seasonal mean SST and precipitation predictions from T126 resolution to 2° and 0.25° , respectively, though this will not affect the results significantly. For the SVD analysis, we use the linearly detrended seasonal mean precipitation and SST during 1982–2007.

Figures 10 and 11 show the homogeneous and heterogeneous correlation maps for the first SVD mode and the global SST or African precipitation, where the areas with p value larger than 0.1 are masked out. For the observation, the first SVD mode only accounts for 13.9%–23.9% of the total covariance, indicating high nonlinearity between the SSTs and precipitation (Figs. 11a–d). CFSv2 has stronger SST–precipitation covariability (19%–30.7%) than the observation for each season, especially for June–August (JJA; Figs. 11e–h). The observation shows that strong correlations between the first SVD mode and SSTs occur over the tropical central and east Pacific consistently across all seasons (Figs. 10a–d), and notable correlations are also found over the tropical Indian and west Pacific during boreal spring (MAM) and fall (SON). Figures 10e–h show that CFSv2 reproduces the ENSO-mode pattern quite well (note the change in sign of Figs. 10f and 10g and Figs. 11f and 11g, but the SST–precipitation covariability remains the same). However, CFSv2 fails to capture the relationship over the tropical South Atlantic during JJA (Figs. 10b,f), which could partly explain the low

predictive skill during the rainy season of WAF (Camberlin et al. 2001). Figure 11 shows that significant correlations between the first SVD mode and African precipitation are constrained to a few local regimes (Figs. 11a–d), but CFSv2 presents stronger coupling over broader areas (Figs. 11e–h). JJA is the rainy season for WAF, and Fig. 11b shows positive correlation over the region. Considering the negative correlation over the Niño-3.4 region (5°N – 5°S , 170° – 120°W ; Fig. 10b), we speculate that an El Niño year has a higher possibility for drought occurrence over WAF during the rainy season. A similar relationship is also found over SAF during December–February (rainy season), for which a warm SST anomaly over the Niño-3.4 region favors drought conditions over the eastern part of SAF. CFSv2 captures those relationships quite well. For the EAF, a La Niña year has a higher possibility for a drought during the short rainy season (SON; Figs. 10, 11). During the long rainy season (MAM), there is no significant correlation between time series of the first SVD SST mode and the EAF precipitation (Fig. 11a), but CFSv2 presents a strong negative correlation (Fig. 11e).

Given the limited large-scale SST–precipitation relationship over Africa at seasonal scales, we may expect other regional atmospheric signals can contribute to the residual portions of the precipitation variance, such as the anomalies in African easterly jet and Saharan northerly wind (Camberlin et al. 2001). Another possible area is the investigation of the predictability derived from the initial land surface anomaly using land

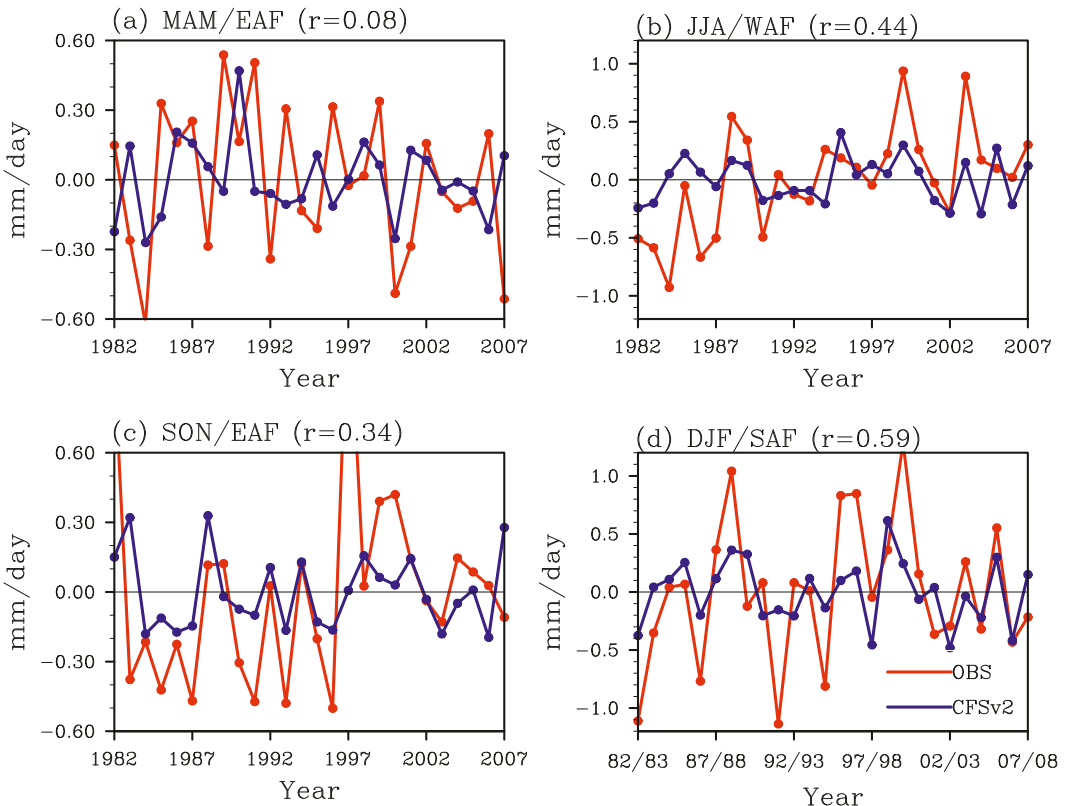


FIG. 9. (a)–(d) Seasonal mean precipitation anomaly averaged over three subdomains for observation and CFSv2 ensemble mean prediction.

surface hydrologic models (Li et al. 2009; Shukla and Lettenmaier 2011). However, the conclusions might be dependent on the land surface model or the parameters of the model. In this study, we collected data from over 800 streamflow gauges to calibrate the VIC model over Africa, but the gauge coverage is far from satisfactory. The uncertainty for the calibrated parameters could influence the characteristics of soil moisture evolution as well as the memory. For example, previous studies found a similar time scale for SPI6 and soil moisture over the United States, while in this study we found the characteristic time for SPI6 and soil moisture could be very different (Fig. 6). Whether the difference comes from the precipitation observation or the hydrologic modeling over Africa, the comparison among different drought indices is made more complicated. Further efforts could be devoted into assimilating more advanced satellite precipitation and soil moisture data to reduce their mismatch and collaborating with local governments to collect more in situ observations. Given the current limitations on observation capability, the use of multiple land surface models (Wang et al. 2009) could be considered to quantify the uncertainty over poorly observed areas.

5. Summary

In this paper, probabilistic drought prediction based on the CFSv2–VIC seasonal hydrologic forecasting system is evaluated over Africa, using SPI6 and soil moisture percentile as drought indices. Compared to climatology, the forecasting system provides more skillful drought prediction out to 3–5 months in terms of BSS, except for soil moisture drought forecast over central Africa. The spatial distribution of BSS for soil moisture is more heterogeneous than that for the SPI6, because the former has more dependency on the geographical variation in soils and vegetation. SPI6 and soil moisture drought forecasts have similar reliability, but the former has higher resolution than the latter, resulting in higher skill out to 4 months over most of the study domain. The analysis of the characteristic time indicates that the spatial difference in predictive skill between SPI6 and soil moisture are correlated well with their difference in persistence. Analysis among different seasons shows that BSS could be as high as 0.8 out to 3 months in the dry season, but drops to as low as 0.3 beyond 1 month in the wet season. This indicates a strong dependency of predictive skill on the seasonality,

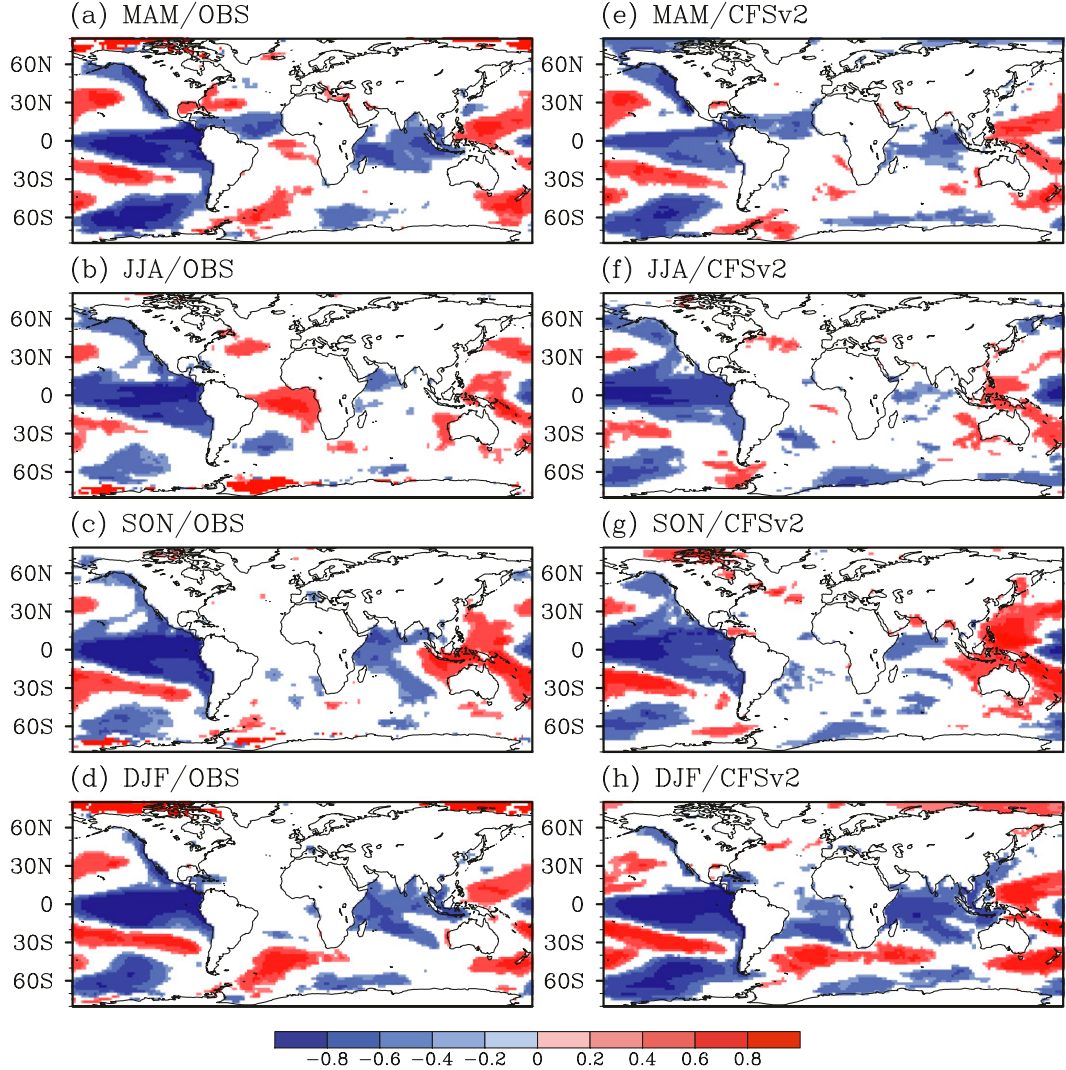


FIG. 10. Homogeneous correlations ($p < 0.1$) between the first SVD SST mode and global SST during 1982–2007 for (a)–(d) observations and (e)–(h) CFSv2 ensemble mean predictions.

especially for WAF and SAF. Although the soil moisture has less persistency than SPI6 over most of the areas in WAF and SAF, it can provide more skillful probabilistic drought forecast than SPI6 at the beginning of the rainy season. With single-number summaries of the forecast performance, the Brier score provides a convenient, quick impression (Wilks 2011); however, further examination should be carried out by assessing the full joint distribution of forecasts and observations. When the system is validated for two extreme drought events in August 1984 and February 1992, low confidence is found even for a 1-month lead forecast, although it performs well in forecasting moderate drought. Actually, the regional mean rainfall anomaly analysis indicates that CFSv2 could not produce the strong

anomaly at seasonal scales for the two extreme cases (Fig. 9).

SVD analysis is used to explore the covariability between African precipitation and global SSTs, and ENSO is found to be the dominant signal for rainy season drought forecast for the west part of WAF and the east part of SAF; CFSv2 reproduces such a relationship quite well. For EAF, there is no significant correlation between the first SVD mode and the precipitation during the long rainy season (MAM) in the observation, but a negative correlation occurred in the CFSv2 forecasts. For the short rainy season (SON), both observation and CFSv2 show that a cold SST anomaly over the Niño-3.4 region seems to contribute to drought in EAF. However, the above SST–precipitation relationship is limited

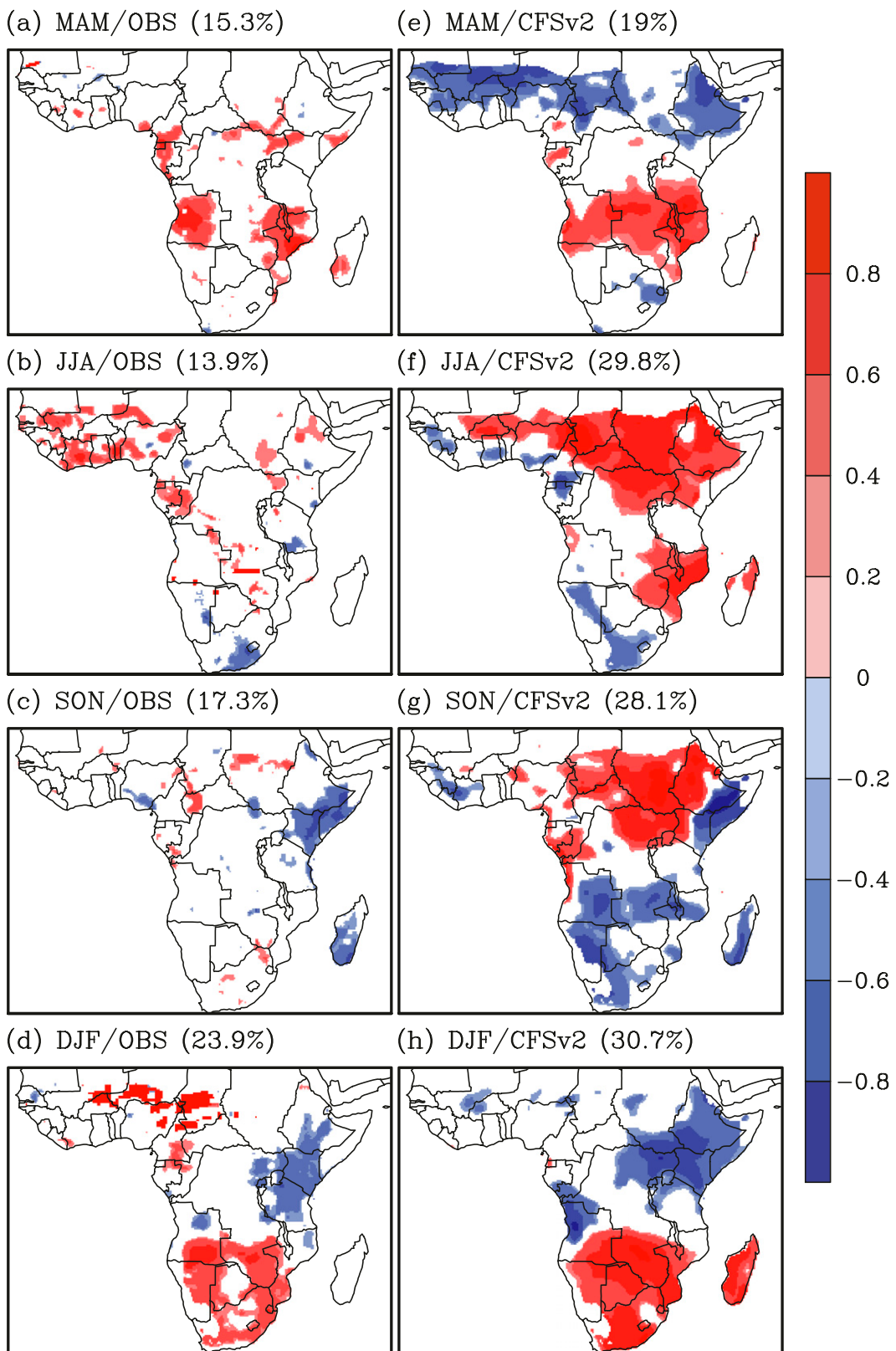


FIG. 11. Heterogeneous correlations ($p < 0.1$) between the first SVD SST mode and African precipitation during 1982–2007 for (a)–(d) observations and (e)–(h) CFSv2 ensemble mean predictions. The numbers in parentheses are their covariances.

because the first SVD mode only accounts for less than 24% of the covariance, although CFSv2 exaggerates it up to 31%. Regional atmospheric and land surface signals need more observational and modeling studies.

Acknowledgments. The research was supported by the NOAA Climate Program Office through Grants NA17RJ2612 and NA10OAR4310246. We thank the anonymous reviewers for their comments. We acknowledge PICSciE/OIT at Princeton University for the supercomputing support.

REFERENCES

- Barnston, A. G., W. Thiao, and V. Kumar, 1996: Long-lead forecasts of seasonal precipitation in Africa using CCA. *Wea. Forecasting*, **11**, 506–520, doi:10.1175/1520-0434(1996)011<0506:LLFOSP>2.0.CO;2.
- , M. K. Tippett, M. L. L'Heureux, S. Li, and D. G. DeWitt, 2012: Skill of real-time seasonal ENSO model predictions during 2002–11: Is our capability increasing? *Bull. Amer. Meteor. Soc.*, **93**, 631–651, doi:10.1175/BAMS-D-11-00111.1.
- Batté, L., and M. Déqué, 2011: Seasonal predictions of precipitation over Africa using coupled ocean-atmosphere general circulation models: Skill of the ENSEMBLES project multi-model ensemble forecasts. *Tellus*, **63A**, 283–299, doi:10.1111/j.1600-0870.2010.00493.x.
- Bowden, J., and F. Semazzi, 2007: Empirical analysis of intra-seasonal climate variability over the Greater Horn of Africa. *J. Climate*, **20**, 5715–5731, doi:10.1175/2007JCLI1587.1.
- Bretherton, C. S., C. Smith, and J. M. Wallace, 1992: An intercomparison of methods for finding coupled patterns in climate data. *J. Climate*, **5**, 541–560, doi:10.1175/1520-0442(1992)005<0541:AIOMFF>2.0.CO;2.
- Camberlin, P., S. Janicot, and I. Poccard, 2001: Seasonality and atmospheric dynamics of the teleconnection between African rainfall and tropical sea-surface temperature: Atlantic vs. ENSO. *Int. J. Climatol.*, **21**, 973–1005, doi:10.1002/joc.673.
- Cook, K. H., 2000: The South Indian Convergence Zone and inter-annual rainfall variability over Southern Africa. *J. Climate*, **13**, 3789–3804, doi:10.1175/1520-0442(2000)013<3789:TSICZA>2.0.CO;2.
- Dutra, E., L. Magnusson, F. Wetterhall, H. L. Cloke, G. Balsamo, S. Boussetta, and F. Pappenberger, 2012: The 2010–2011 drought in the Horn of Africa in ECMWF reanalysis and seasonal forecast products. *Int. J. Climatol.*, **33**, 1720–1729, doi:10.1002/joc.3545.
- Gimeno, L., and Coauthors, 2012: Oceanic and terrestrial sources of continental precipitation. *Rev. Geophys.*, **50**, RG4003, doi:10.1029/2012RG000389.
- Hoerling, M., and A. Kumar, 2003: The perfect ocean for drought. *Science*, **299**, 691–694, doi:10.1126/science.1079053.
- Hoskins, B. J., and D. Karoly, 1981: The steady linear response of a spherical atmosphere to thermal and orographic forcing. *J. Atmos. Sci.*, **38**, 1179–1196, doi:10.1175/1520-0469(1981)038<1179:TSLROA>2.0.CO;2.
- Landman, W. A., D. DeWitt, D. Lee, A. Beraki, and D. Lotter, 2012: Seasonal rainfall prediction skill over South Africa: One- versus two-tiered forecasting systems. *Wea. Forecasting*, **20**, 5715–5731.
- Li, H., L. Luo, E. F. Wood, and J. Schaake, 2009: The role of initial conditions and forcing uncertainties in seasonal hydrologic forecasting. *J. Geophys. Res.*, **114**, D04114, doi:10.1029/2008JD010969.
- Liang, X., E. F. Wood, and D. P. Lettenmaier, 1996: Surface soil moisture parameterization of the VIC-2L model: Evaluation and modifications. *Global Planet. Change*, **13**, 195–206, doi:10.1016/0921-8181(95)00046-1.
- Luo, L., and E. F. Wood, 2007: Monitoring and predicting the 2007 U.S. drought. *Geophys. Res. Lett.*, **34**, L22702, doi:10.1029/2007GL031673.
- , —, and M. Pan, 2007: Bayesian merging of multiple climate model forecasts for seasonal hydrological predictions. *J. Geophys. Res.*, **112**, D10102, doi:10.1029/2006JD007655.
- Mason, S. J., 1998: Seasonal forecasting of South African rainfall using a non-linear discriminant analysis model. *Int. J. Climatol.*, **18**, 147–164, doi:10.1002/(SICI)1097-0088(199802)18:2<147::AID-JOC229>3.0.CO;2-6.
- McCabe, G. J., M. A. Palecki, and J. L. Betancourt, 2004: Pacific and Atlantic Ocean influences on multidecadal drought frequency in the United States. *Proc. Natl. Acad. Sci. USA*, **101**, 4136–4141, doi:10.1073/pnas.0306738101.
- McKee, T. B., N. J. Doesken, and J. Kleist, 1993: The relationship of drought frequency and duration to time scales. Preprints, *Eighth Conf. on Applied Climatology*, Anaheim, CA, Amer. Meteor. Soc., 179–184.
- , —, and —, 1995: Drought monitoring with multiple time scale. Preprints, *Ninth Conf. on Applied Climatology*, Dallas, TX, Amer. Meteor. Soc., 233–236.
- Mo, K., S. Shukla, D. P. Lettenmaier, and L. Chen, 2012: Do Climate Forecast System (CFSv2) forecasts improve seasonal soil moisture prediction? *Geophys. Res. Lett.*, **39**, L23703, doi:10.1029/2012GL053598.
- Peterson, T. C., P. A. Stott, and S. Herring, 2012: Explaining extreme events of 2011 from a climate perspective. *Bull. Amer. Meteor. Soc.*, **93**, 1041–1067, doi:10.1175/BAMS-D-12-00021.1.
- Pozzi, W., and Coauthors, 2013: Towards global drought early warning capability: Expanding international cooperation for the development of a framework for global drought monitoring and forecasting. *Bull. Amer. Meteor. Soc.*, **94**, 776–785, doi:10.1175/BAMS-D-11-00176.1.
- Saha, S., and Coauthors, 2013: The NCEP Climate Forecast System version 2. *J. Climate*, in press.
- Schubert, S. D., M. J. Suarez, P. J. Pegion, R. D. Koster, and J. T. Bacmeister, 2004: Causes of long-term drought in the U.S. Great Plains. *J. Climate*, **17**, 485–503, doi:10.1175/1520-0442(2004)017<0485:COLDIT>2.0.CO;2.
- , and Coauthors, 2009: A U.S. CLIVAR project to assess and compare the responses of global climate models to drought-related SST forcings patterns: Overview and results. *J. Climate*, **22**, 5251–5272, doi:10.1175/2009JCLI3060.1.
- Sheffield, J., and E. F. Wood, 2011: *Drought: Past Problems and Future Scenarios*. Earth Ltd., 210 pp.
- , G. Goteti, and E. F. Wood, 2006: Development of a 50-yr high-resolution global dataset of meteorological forcings for land surface modeling. *J. Climate*, **19**, 3088–3111, doi:10.1175/JCLI3790.1.
- , K. M. Andreas, E. F. Wood, and D. P. Lettenmaier, 2009: Global and continental drought in the second half of the twentieth century: Severity-area-duration analysis and temporal variability of large-scale events. *J. Climate*, **22**, 1962–1981, doi:10.1175/2008JCLI2722.1.
- Shukla, S., and D. P. Lettenmaier, 2011: Seasonal hydrologic prediction in the United States: Understanding the role of

- initial hydrologic conditions and seasonal climate forecast skill. *Hydrol. Earth Syst. Sci.*, **15**, 3529–3538, doi:10.5194/hess-15-3529-2011.
- Smith, D. M., A. A. Scaife, and B. P. Kirtman, 2012: What is the current state of scientific knowledge with regard to seasonal to decadal forecasting. *Environ. Res. Lett.*, **7**, 015602, doi:10.1088/1748-9326/7/1/015602.
- Smith, T. M., R. W. Reynolds, T. C. Peterson, and J. Lawrimore, 2008: Improvements to NOAA's historical merged land-ocean surface temperature analysis (1880–2006). *J. Climate*, **21**, 2283–2296, doi:10.1175/2007JCLI2100.1.
- Svoboda, M., and Coauthors, 2002: The Drought Monitor. *Bull. Amer. Meteor. Soc.*, **83**, 1181–1190.
- Tarhule, A., and P. J. Lamb, 2003: Climate research and seasonal forecasting for West Africans: Perceptions, dissemination, and use? *Bull. Amer. Meteor. Soc.*, **84**, 1741–1759, doi:10.1175/BAMS-84-12-1741.
- Trenberth, K. E., 1984: Some effects of finite sample size and persistence on meteorological statistics. Part II: Potential predictability. *Mon. Wea. Rev.*, **112**, 2369–2379, doi:10.1175/1520-0493(1984)112<2369:SEOFSS>2.0.CO;2.
- , and J. M. Caron, 2000: The Southern Oscillation revisited: Sea level pressures, surface temperatures and precipitation. *J. Climate*, **13**, 4358–4365, doi:10.1175/1520-0442(2000)013<4358:TSORSL>2.0.CO;2.
- Wallace, J. M., C. Smith, and C. S. Bretherton, 1992: Singular value decomposition of wintertime sea-surface temperature and 500-mb height anomalies. *J. Climate*, **5**, 561–576, doi:10.1175/1520-0442(1992)005<0561:SVDOWS>2.0.CO;2.
- Wang, A., T. J. Bohn, S. P. Mahanama, R. D. Koster, and D. P. Lettenmaier, 2009: Multimodel ensemble reconstruction of drought over the continental United States. *J. Climate*, **22**, 2694–2712, doi:10.1175/2008JCLI2586.1.
- Wilks, D. S., 2011: *Statistical Methods in the Atmospheric Sciences*. 3rd ed. International Geophysics Series, Vol. 100, Academic Press, 676 pp.
- Yoon, J. H., K. Mo, and E. F. Wood, 2012: Dynamic-model-based seasonal prediction of meteorological drought over the contiguous United States. *J. Hydrometeor.*, **13**, 463–481, doi:10.1175/JHM-D-11-038.1.
- Yuan, X., E. F. Wood, L. Luo, and M. Pan, 2011: A first look at Climate Forecast System version 2 (CFSv2) for hydrological seasonal prediction. *Geophys. Res. Lett.*, **38**, L13402, doi:10.1029/2011GL047792.
- , —, J. K. Roundy, and M. Pan, 2013: CFSv2-based seasonal hydroclimatic forecasts over conterminous United States. *J. Climate*, **26**, 4828–4847, doi:10.1175/JCLI-D-12-00683.1.